Percolation-based model for tunneling conductivity in systems of partially aligned cylinders

Avik P. Chatterjee[*]

Department of Chemistry, SUNY College of Environmental Science and Forestry, One Forestry Drive, Syracuse, New York 13210, USA

A model is developed for anisotropies in the conductivity in monodisperse systems of uniaxially aligned cylindrical fibers. Concepts from percolation theory (specifically, a lattice approach toward describing percolation by rods with large aspect ratios) are unified with a simple picture based upon resistors combined in series and parallel to calculate the conductivities in fiber-based nanocomposites in directions that are longitudinal and transverse with respect to the axis of particle alignment. Results obtained for three different orientational distribution functions (ODFs) reveal a peak in the dependence of the longitudinal conductivity upon mean orientational order parameter ($\langle S \rangle$), qualitatively similar to findings that have been reported from computer simulations. In contrast, the transverse conductivity decreases monotonically with increasing values of $\langle S \rangle$ for each of the ODFs investigated.

I. INTRODUCTION

Percolation phenomena play a central role in the structure and organization of complex networks in both physical (tangible) [1–4] and social contexts [5–7]. For composite materials, mechanical as well as transport properties are strongly influenced by the formation of networks (defined by physical proximity) of particles that provide rigidity and/or pathways for thermal or electrical conductivity [8–12]. In systems that contain elongated particles that have varying degrees of alignment (that can be achieved through conditions of applied external fields or rheological flow), the distribution function over orientations provides a variable in addition to the volume fraction (or composition) and particle aspect ratio that characterizes the state of dispersion [13,14]. Experiments as well as computer simulations reveal that, for systems containing rodlike particles with varying degrees of uniaxial orientational alignment embedded within an insulating matrix, strong anisotropies can develop between conductivities measured along directions longitudinal and transverse with respect to the alignment direction [15–20]. Such studies have reported an interesting nonmonotonicity in the dependence of the longitudinal conductivity upon the mean orientational order parameter $\langle S \rangle$, such that there appears an optimum degree of alignment at which the conductivity is maximized [15,16,19,20]. The present work develops a theoretical model for the conductivity in such partially oriented fiber-based nanocomposites, in which the longitudinal and transverse (or, parallel and perpendicular) conductivities are calculated as functions of the particle aspect ratio and volume fraction, the length scale characterizing electron tunneling between rods, the resistance between rods at contact and the lineal fiber resistivity, and the orientational distribution function (ODF).

Our starting point is a lattice model for percolation in systems of rodlike particles that has been generalized to treat systems with varying degrees of uniaxial alignment [21,22]. This formalism neglects contributions from closed loops and assumes treelike interparticle connectivity, and we further assume that the spatial distribution of particles is random and homogeneous. The matrix is assumed to be perfectly insulating. For given specifications of the volume fraction, aspect ratio (for simplicity we consider the particles to be of uniform size and shape, that is, monodisperse), and ODF, this formalism enables us to identify the soft-shell thickness or connectedness range that permits the particles to achieve percolation. This estimate is combined with a simple model of resistors in series and parallel to calculate the direction-dependent conductivity. Electron transport through the material is assumed to follow a sequence of (i) travel along the direction of a fiber between points of contact with neighboring rods, and (ii) tunneling jumps at such points of proximity from one rod to the next. Reminiscent of the critical path approximation (CPA) [23], the conductance associated with each tunneling step is estimated by assigning to each such step a distance equal to the critical surface-to-surface separation that enforces the percolation threshold condition for given values of the remaining variables in the problem. This modeling framework unifies ideas drawn from percolation theory with existing approaches that have utilized combinations of series and parallel resistors to characterize anisotropic conductivities [24–26]. It should be noted that for isotropic systems of elongated particles, percolation thresholds can also be calculated within an integral equation–based formalism [27–29].

The remainder of this paper is organized in the following way. Sections II A–II C present our model for percolation and the connectedness distance; calculation of the longitudinal and transverse conductivities; and, the orientational averages of a number of circular functions that are required to complete the calculation, for three different choices for the ODF, respectively. Results from calculations based upon our model are presented in Sec. III, followed by conclusions in Sec. IV.

_____

[*]apchatte@esf.edu

II. LATTICE MODEL FOR PERCOLATION AND CONDUCTIVITY IN SYSTEMS OF PARTIALLY ALIGNED MONODISPERSE RODS

A. Model for percolation in partially aligned systems of rods

We begin by presenting our model for percolation in monodisperse systems of cylindrical rods the long axes of which are partially aligned along a prescribed direction, which we denote the z axis. The length and radius of the nonoverlapping cores of the rods are assumed to be uniform, and are denoted L and R, respectively, and the centers of the rods are assumed to be distributed in a spatially random manner. The aspect ratio, defined as L/R, is assumed to always be much larger than unity and the rod number density and core-occupied volume fraction, denoted ρ and φ, respectively, are related by $\phi = \pi \rho R^2 L$. The impenetrable core of each individual particle is envisioned as being surrounded by a larger coaxial cylinder with length and radius equal to $L + 2\lambda$ and $R + \lambda$, respectively, that represents a combined core-plus-shell object, and a contact is defined to exist between a pair of cylinders if an overlap occurs between their penetrable shells (of lengths $L + 2\lambda$ and radii $R + \lambda$). This length scale λ thus defines the connectedness range for particle pairs. At each such contact between a pair of rods, the tunneling conductance is approximated by $\sigma(r) \approx (e^{-2r/\xi})/\rho_0$, where (i) ρ_0 represents the contact resistance between a pair of rods that touch each other directly, (ii) the shortest distance between the surfaces of the impenetrable cores of the pair of particles is denoted r, and (iii) the tunneling length scale ξ is typically in the range $0.1\,\text{nm} \leqslant \xi \leqslant 10\,\text{nm}$ [30]. The present work neglects the dependence of the tunneling resistance upon the relative angle between the pair of rods [31], and assumes that $\sigma(r)$ depends solely upon the separation between particle surfaces at the point of adjacency.

For the case of a random spatial distribution of the particles, the expected average number of contacts experienced by one rod, denoted $\langle n \rangle$, equals [32]

$$\langle n \rangle = \rho \, \delta \, V_{\text{exc}}, \tag{1}$$

where δV_{exc} is the appropriate orientationally averaged difference in excluded volumes between the core-plus-shell, and core-only, regions for a pair of particles. (The "excluded volume" refers to the volume that is denied to the center of a second particle by virtue of the constraint that the impenetrable cores of a pair of particles are not permitted to overlap). The orientational distribution function (ODF) for the rods, denoted $f(\theta)$, is normalized such that $\int_0^\pi d\theta \sin(\theta) f(\theta) = 1$, where θ denotes the angle between the axis of a rod and the orientation direction (z axis). Our model assumes that the ODF that depends only upon θ is independent of the azimuthal angle φ.

The problem of percolation in this continuum representation can be mapped onto a lattice analog by considering a treelike Bethe lattice in which particles are represented by occupied sites, and where vacant lattice sites represent locations where particles are added as the volume fraction rises [21]. Closed loops are entirely neglected and the lattice is assumed to be treelike. The number of links (or, equivalently, bonds or edges) that emerge from each site, referred to as the vertex degree, is denoted Z. (We use the uppercase symbol Z to denote the vertex degree; the lowercase symbol z is reserved for the appropriate direction in a Cartesian coordinate system). If we assume that (i) the occupation probability for a randomly selected lattice site equals the core-occupied volume fraction φ, and that (ii) the average number of contacts per particle $\langle n \rangle$ (continuum picture) equals that for an occupied site (lattice picture), we find that $Z_c = \rho \delta V_{\text{exc}}/\phi = \delta V_{\text{exc}}/\pi R^2 L$. These relations, when combined together with the appropriate expression for the excluded volume [33] averaged over the appropriate ODF, lead to

$$Z = \frac{4\lambda}{\pi L} \left[\begin{array}{c} \frac{\pi(6-\pi)}{2(\pi-2)} \left\{ \frac{L}{R}\left(2 + \frac{\lambda}{R}\right) + 2\left(1 + \frac{\lambda}{R}\right)^2 \right\} \\ + \left[\begin{array}{c} \pi \left\{ \left(\frac{\lambda}{R}\right)^2 + \frac{3\lambda}{R} + 3 \right\} \\ + \frac{(\pi^2 - 2\pi - 4)}{(\pi-2)} \left\{ \frac{L}{R}\left(2 + \frac{\lambda}{R}\right) + 2\left(1 + \frac{\lambda}{R}\right)^2 \right\} \\ + \left\{ 4\left(\frac{L}{R} + \frac{\lambda}{R}\right) + \left(\frac{L}{R} + \frac{2\lambda}{R}\right)^2 \right\} \end{array} \right] \langle |\sin(\gamma)| \rangle \\ + \frac{\pi(5\pi-14)}{2(\pi-2)} \left\{ \frac{L}{R}\left(2 + \frac{\lambda}{R}\right) + 2\left(1 + \frac{\lambda}{R}\right)^2 \right\} \langle |\cos(\gamma)| \rangle \end{array} \right], \tag{2}$$

where γ denotes the relative angle between the axes of a pair of rods and the symbol $\langle \cdots \rangle$ indicates an average taken over the ODF. In order to obtain the closed-form expression in Eq. (2), we have used an accurate interpolation [34] in terms of $\sin(\gamma)$ and $\cos(\gamma)$ for the complete elliptic integral of the second kind that appears in the result for the excluded volume between a pair of rods [33].

For the assumed treelike arrangement of particles on a Bethe lattice where closed loops are neglected, the percolation threshold condition is [1,35]

$$\phi_c[Z_c(\lambda_c, L, R)] = 1. \tag{3}$$

Taken together, Eqs. (2) and (3) may be interpreted either (i) to determine the critical volume fraction ϕ_c at which percolation ensues (that is, there first appears a connected cluster of infinite extent) for a fixed value of λ, or (ii) to ascertain the critical connectedness length scale λ_c at which percolation ensues for given values of L, R, and the volume fraction ϕ. The latter interpretation and usage are adopted in our present work. When the threshold condition is precisely satisfied (that is, right at the percolation threshold) the average number of contacts that a randomly selected rod experiences with all of the other rods in the system, denoted $\langle n_c \rangle$, satisfies $\langle n \rangle_c = Z_c/(Z_c - 1) = 1 + \phi$.

An auxiliary quantity that will be useful for our subsequent development is the average of $1/(n + 1)$, where n denotes the number of contacts per rod, evaluated at the percolation threshold and only for those rods that experience two or more contacts with other particles. Under the assumption that the number of contacts per rod follows a Poisson distribution with an average value denoted $\langle n \rangle$, it can be shown that this required average (which we denote ε) is given by

$$\varepsilon = \left\langle \frac{1}{n+1} \right\rangle_{n \geqslant 2} = \frac{\left[1 - \left\{ 1 + \langle n \rangle + \frac{\langle n \rangle^2}{2} \right\} e^{-n} \right]}{\langle n \rangle \left[1 - \{1 + \langle n \rangle\} e^{-n} \right]}. \quad (4)$$

If the connectedness length scale λ is chosen to enforce the percolation threshold requirement (that is, $\lambda = \lambda_c$) for vanishingly small volume fractions (that is, as $\phi \rightarrow 0$), we find that $\langle n \rangle_c \rightarrow 1$ and $\varepsilon \approx 0.303\,89$.

B. Calculation of the longitudinal and transverse conductivities

This section presents our method for estimating the conductivities along longitudinal (z) and transverse (x) directions for uniaxially aligned systems of rods. Our calculation combines ideas from percolation theory as well as an admittedly heuristic and simple model of series and parallel combinations of resistors [24–26].

We start by considering a cube of the composite material with each side of length denoted A, oriented such that the direction of particle alignment (z) is parallel to one of the sets of edges of the cube. For generality, we examine the case of an electric field applied along the α direction (where $\alpha = x$, y, or z), and the resultant current or charge transport across faces of the cube each perpendicular to the α direction, parallel to each other, and of surface area A^2. Our model breaks up the calculation of the net resistance across the faces of the cube into two parts:

(i) We envision the path of an electron as a sequence of steps in the direction of the applied field, with each individual step being comprised of two parts: (a) travel along the fiber axis between a pair of rod-rod contacts, followed by (b) a tunneling jump by way of a rod-rod contact location to another rod. We first combine the resistances from a chain of such events that span the sample cube additively, as resistors in series.

(ii) We next estimate the number of such chains or pathways that span the sample cube, and combine the cumulative resistance of each such chain [obtained from step (i)] as if these are now resistors arranged in parallel.

Our calculation proceeding along the above sequence of steps is discussed next.

For simplicity, and in keeping with the spirit of the critical path approximation, we assume that each tunneling event between a pair of rods crosses a distance equal to $2\lambda_c$ between the surface of one rod and the next, where λ_c is the soft-shell thickness that satisfies the percolation threshold condition for the given values of L, R, and ϕ. With the additional assumption that such tunneling jumps are distributed with forward-hemispherical symmetry in the direction of the applied field (that is, are oriented randomly in the hemispherical region that corresponds to the field direction), we find that the typical distance traveled per tunneling event in the field direction is

$\approx \lambda_c$. The projected distance along the α direction between the extremities of a cylindrical rod is easily verified to be equal to $L|\cos(\theta_\alpha)| + 2R|\sin(\theta_\alpha)|$, where θ_α is the angle between the rod axis and the α direction; this quantity, multiplied by ε [from Eq. (4)] and averaged over the ODF, provides an estimate for the typical distance traveled along the fiber axis, projected onto the field direction, between tunneling jumps from rod to rod. [Our calculation of ε in Eq. (4) attempts to crudely account for the fact that for a rod to not be a dead end for charge transport, it should have at least two contacts with other particles.] Each individual transit along the axis of a rod, followed by tunneling to another rod, thus leads to an average displacement $\langle l_\alpha \rangle$ in the field direction:

$$\langle l_\alpha \rangle \approx \varepsilon \left[L \langle |\cos(\theta_\alpha)| \rangle + 2R \langle |\sin(\theta_\alpha)| \rangle \right] + \lambda_c. \quad (5)$$

The number of such events that are required to traverse the distance between opposite faces of the cube may be estimated as $\approx A / \langle l_\alpha \rangle$. Treating these steps as resistors that may be combined in series yields the following estimate for the resistance r_α of one such pathway between sides of the cube:

$$r_\alpha \approx \frac{A}{\langle l_\alpha \rangle} [\rho_f L \varepsilon + \rho_0 e^{4\lambda_c/\xi}], \quad (6)$$

where ρ_f denotes the resistance per unit length or lineal resistance (in units of $\Omega\,\mathrm{m}^{-1}$) along the axis of a fiber.

In order to estimate the number of such pathways linking opposite faces of the cube, we equate this to the expected number of intersections $\langle N_\alpha \rangle$ between a plane surface of area A^2 that is normal to the α direction and rods in the system. (This hypothetical surface is assumed to freely penetrate the cores of the particles if necessary.) For this step of the calculation we augment each rod with a shell of thickness equal to half the tunneling range; that is, we perform the replacements $R \rightarrow R + \xi/2$, $L \rightarrow L + \xi$, to account for the fact that the tunneling probability does not diminish to zero immediately upon crossing the boundary of the particle. An otherwise insulating matrix containing point particles for which both L and R vanish, but that have a nonvanishing, finite value for ξ, would still exhibit conductive paths and nonzero conductivity due to tunneling effects. The number of such fiber-surface crossings is [36]

$$\langle N_\alpha \rangle \approx \left(\frac{\phi}{\pi} \right) \left(\frac{A}{R} \right)^2 \left[\left(1 + \frac{\xi}{L} \right) \langle |\cos(\theta_\alpha)| \rangle \right.$$
$$\left. + \left(\frac{2R}{L} + \frac{\xi}{L} \right) \langle |\sin(\theta_\alpha)| \rangle \right]. \quad (7)$$

The combination in parallel of $\langle N_\alpha \rangle$ conductive pathways each with resistance r_α, followed by accounting for the edge length of the cube (set equal to A initially), leads to the following result for the conductance σ_α measured along the α direction:

$$\sigma_\alpha \approx \frac{\langle N_\alpha \rangle}{A\, r_\alpha}. \quad (8)$$

Equations (5)–(8) lead to the following expressions that have been written in dimensionless form:

$$R \, \rho_0 \, \sigma_\alpha \approx \left(\frac{\phi}{\pi}\right) \left[\frac{\left[\varepsilon \left\{ \left(\frac{L}{R}\right) \langle \, | \cos(\theta_\alpha)| \rangle + 2 \langle \, | \sin(\theta_\alpha) \rangle \right\} + \frac{\lambda_c}{R} \right]}{\left[\left(\frac{\rho_f R}{\rho_0}\right) \left(\frac{L}{R}\right) \varepsilon + e^{4 \, \lambda_c/\xi} \right]} \right]$$

$$\times \left[\left(1 + \frac{\xi}{L}\right) \langle | \cos(\theta_\alpha)| \rangle + \left(\frac{2R}{L} + \frac{\xi}{L}\right) \langle | \sin(\theta_\alpha)| \rangle \right]. \tag{9}$$

The choices $\alpha = z$ and $\alpha = x$ in Eq. (9) yield results for the longitudinal (parallel, $\sigma_\parallel$) and transverse (perpendicular, $\sigma_\perp$) conductivities, respectively, and the anisotropy ratio ($\sigma_\parallel/\sigma_\perp = \sigma_z/\sigma_x$) can be expressed as

$$\frac{\sigma_z}{\sigma_x} \approx \left[\frac{\left\{ \varepsilon \left[\left(\frac{L}{R}\right) \langle | \cos(\theta_z)| \rangle + 2 \langle | \sin(\theta_z)| \rangle \right] + \frac{\lambda_c}{R} \right\}}{\left\{ \varepsilon \left[\left(\frac{L}{R}\right) \langle | \cos(\theta_x)| \rangle + 2 \langle | \sin(\theta_x)| \rangle \right] + \frac{\lambda_c}{R} \right\}} \right] \left[\frac{\left(1 + \frac{\xi}{L}\right) \langle | \cos(\theta_z)| \rangle + \left(\frac{2R}{L} + \frac{\xi}{L}\right) \langle | \sin(\theta_z)| \rangle}{\left(1 + \frac{\xi}{L}\right) \langle | \cos(\theta_x)| \rangle + \left(\frac{2R}{L} + \frac{\xi}{L}\right) \langle | \sin(\theta_x)| \rangle} \right]. \tag{10}$$

It bears noting that the combination of variables $\rho_f R/\rho_0$ that appears in Eq. (9) is a dimensionless quantity.

C. Orientational distribution functions (ODFs) and angular averages

This section describes three different choices for the ODF and the associated averages over circular functions that are required to calculate the longitudinal and transverse conductivities from Eq. (10). The average of the traditional orientational order parameter, denoted $\langle S \rangle$, is given by

$$\langle S \rangle = \left\langle \frac{3\cos^2\theta_z - 1}{2} \right\rangle = \int_0^\pi d\theta_z \sin(\theta_z) \, f(\theta_z) \left[\frac{3\cos^2(\theta_z) - 1}{2} \right]. \tag{11}$$

The standard deviation in the orientational order parameter, denoted σ_S, is defined by way of the relation $\sigma_S^2 = \langle S \rangle^2 - \langle S \rangle^2$. The ODFs described below are subsequently referred to as simply ODFs numbered (i), (ii), and (iii), respectively.

1. ODF with σ_S equal to zero (i)

We first consider an ODF for which σ_S is equal to zero for the prescribed value of $\langle S \rangle$. In this case, the ODF reduces to a Dirac delta function located at $\theta_0 = \theta_z$, where

$$\cos(\theta_0) = \sqrt{(1 + 2 \langle S \rangle)/3}. \tag{12}$$

For this ODF, the required orientational averages are given by

$$\langle |\cos(\theta_z)| \rangle = \cos(\theta_0), \quad \langle | \sin(\theta_z)| \rangle = \sqrt{2 (1 - \langle S \rangle)/3}, \tag{13}$$

$$\langle | \cos(\theta_x)| \rangle = 2 \sin(\theta_0)/\pi, \tag{14}$$

and

$$\langle | \sin(\theta_x)| \rangle = \frac{[\pi(4 - \pi) + (\pi^2 - 2\pi - 4)\sin(\theta_0) + 2\pi(\pi - 3)\cos(\theta_0)]}{\pi(\pi - 2)}, \tag{15}$$

where the interpolation introduced in Eq. (3) of Ref. [22] for the complete elliptic integral of the second kind has been used in expressing the average $\langle | \sin(\theta_x)| \rangle$. The averages $\langle | \sin(\gamma)| \rangle$ and $\langle | \cos(\gamma)| \rangle$ required for use in conjunction with Eq. (2) are in this case given by

$$\langle | \sin(\gamma)| \rangle = \frac{2}{\pi} \left(\sin(\theta_0) + \cos^2(\theta_0) \left\{ \ln \left[\tan(\theta_0) + \frac{1}{\cos(\theta_0)} \right] \right\} \right), \tag{16}$$

$$\langle | \cos(\gamma)| \rangle = \cos^2(\theta_0) \quad \text{if } \langle S \rangle \leqslant 1/4, \tag{17}$$

and

$$\langle | \cos(\gamma)| \rangle = \left(\frac{4 x_0}{\pi} - 1 \right) \cos^2(\theta_0) + \frac{2 \sqrt{2\sin^2(\theta_0) - 1}}{\pi}, \quad \text{if } \langle S \rangle > 1/4, \tag{18}$$

where $x_0 = \sin^{-1}[1/\sqrt{2} \sin \theta_0]$.

2. ODF with σ_S maximized for each given value of $\langle S \rangle$ (ii)

We consider next an ODF that comprises a linear combination of a pair of Dirac delta functions located at $\theta_0 = 0$ and at $\theta_0 = \pi/2$, with weight factors that reproduce a prescribed value of $\langle S \rangle$. This ODF ought to represent the maximum possible value for σ_S for each given value of $\langle S \rangle$. The required averages in this case are given by

$$\langle |\cos(\theta_z)| \rangle = (1 + 2\langle S \rangle)/3, \quad \langle |\sin(\theta_z)| \rangle = 2(1 - \langle S \rangle)/3,$$
(19)

$$\langle |\cos(\theta_x)| \rangle = 4(1 - \langle S \rangle)/3\pi,$$
(20)

and

$$\langle |\sin(\theta_x)| \rangle = \frac{[\pi(1 + 2\langle S \rangle) + 4(1 - \langle S \rangle)]}{3\pi}.$$
(21)

The averages $\langle |\sin(\gamma)| \rangle$ and $\langle |\cos(\gamma)| \rangle$ required for use in conjunction with Eq. (2) are in this case given by

$$\langle |\sin(\gamma)| \rangle = \frac{4(1 - \langle S \rangle)}{9\pi} [\pi + 2 + 2(\pi - 1)\langle S \rangle], \quad (22)$$

and

$$|\cos(\gamma)| = \frac{1}{9\pi} [\pi + 8 + 4(\pi - 4)S + 4(\pi + 2)S^2].$$
(23)

It bears emphasis that for ODFs (i) and (ii), setting $\langle S \rangle = 0$ does *not* correspond to the case of a fully isotropic orientational distribution.

3. Step function ODF (iii)

As our third and final example, we consider a step function ODF that has been employed in a number of existing computer simulation studies [19,20,37] of systems of partially aligned rods:

$$f(\theta_z) = \frac{1}{2[1 - \cos(\beta)]}, \quad \text{for } 0 \leqslant \theta_z \leqslant \beta,$$
$$\text{and} \quad \pi - \beta \leqslant \theta_z \leqslant \pi,$$
$$\text{and} \quad f(\theta_z) = \text{zero, otherwise.}$$
(24)

Setting β equal to $\pi/2$ and zero corresponds to fully isotropic and perfectly aligned orientational distributions, respectively. For this ODF, it can be readily shown that

$$\langle S \rangle = \cos(\beta)[1 + \cos(\beta)]/2,$$
(25)

and

$$\langle S^2 \rangle = \frac{1}{5} \left\{ 1 - \frac{\cos(\beta)[1 + \cos(\beta)][1 - 9\cos^2(\beta)]}{4} \right\}.$$
(26)

The required averages in this case are given by

$$\langle |\cos(\theta_z)| \rangle = \cos^2(\beta/2),$$
$$\langle |\sin(\theta_z)| \rangle = \frac{[\beta - \sin(\beta)\cos(\beta)]}{2[1 - \cos(\beta)]},$$
(27)

$$\langle |\cos(\theta_x)| \rangle = [\beta - \sin(\beta)\cos(\beta)]/\pi[1 - \cos(\beta)], \quad (28)$$

and

$$\langle |\sin(\theta_x)| \rangle = \frac{2}{\pi(\pi - 2)} \left\{ \frac{\pi(4 - \pi)}{2} + \frac{(\pi^2 - 2\pi - 4)}{8\sin^2(\beta/2)} \right.$$
$$\left. \times [\beta - \sin(\beta)\cos(\beta)] + \pi(\pi - 3)\cos^2(\beta/2) \right\},$$
(29)

where the interpolation introduced in Ref. [22] for the complete elliptic integral of the second kind has been used in expressing the average $\langle |\sin(\theta_x)| \rangle$.

The averages $\langle |\sin(\gamma)| \rangle$ and $\langle |\cos(\gamma)| \rangle$ for this ODF are estimated by interpolating between the results from the first and second ODFs, (i) and (ii), considered above using $\sigma_S/\sigma_S^{\max}$ as the interpolation variable, where σ_S is calculated from Eqs. (25) and (26) and $\sigma_S^{\max}$ is calculated from the case of ODF (ii) (above) for the given value of $\langle S \rangle$. [It can be shown that $\sigma_S^{\max} = \sqrt{(1 - \langle S \rangle)(1 + 2\langle S \rangle)/2}$]. Our interpolation takes the form

$$\langle |\sin(\gamma)| \rangle = \langle |\sin(\gamma)| \rangle_1$$
$$+ \left(\frac{\sigma_S}{\sigma_S^{\max}} \right) \left[\frac{\sigma_S}{\sigma_S^{\max}} + a_1 \left(1 - \frac{\sigma_S}{\sigma_S^{\max}} \right) \right]$$
$$\times [\langle |\sin(\gamma)| \rangle_2 - \langle |\sin(\gamma)| \rangle_1], \quad (30)$$

and

$$|\cos(\gamma)| = |\cos(\gamma)|_1 + \left(\frac{\sigma_S}{\sigma_S^{\max}} \right) \left[\frac{\sigma_S}{\sigma_S^{\max}} + a_2 \left(1 - \frac{\sigma_S}{\sigma_S^{\max}} \right) \right]$$
$$\times [|\cos(\gamma)|_2 - |\cos(\gamma)|_1], \quad (31)$$

where the subscripts 1 and 2 refer to the results reported previously for ODFs (i) and (ii). The forms selected for Eqs. (30) and (31) reduce (by construction) to the results for ODFs (i) and (ii) when σ_S equals either zero or $\sigma_S^{\max}$, respectively, for any value of $\langle S \rangle$. The coefficients a_1 and a_2 are chosen in order to enforce agreement with the results for the fully isotropic situation with $\langle S \rangle = 0$, for which it is known that $\sigma_S^{\mathrm{iso}} = 1/\sqrt{5}$, $\langle |\sin(\gamma)| \rangle_{\mathrm{iso}} = \pi/4$, and $\langle |\cos(\gamma)| \rangle_{\mathrm{iso}} = 1/2$. In the interests of completeness it should be noted that for an isotropic system $\langle |\sin(\theta)| \rangle_{\mathrm{iso}} = \pi/4$ and $\langle |\cos(\theta)| \rangle_{\mathrm{iso}} = 1/2$, regardless of direction.

It bears reiteration that setting $\langle S \rangle = 0$ leads to the fully isotropic orientational distribution only for ODF (iii). This is reflected in the fact that when $\langle S \rangle = 0$, for ODFs (i), (ii), and (iii), the standard deviation σ_S equals zero, $1/\sqrt{2}$, and $1/\sqrt{5}$, respectively.
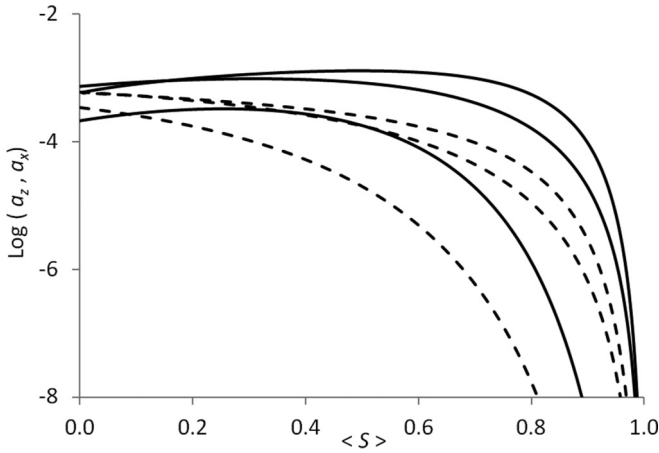
FIG. 1. The nondimensionalized longitudinal and transverse conductivities a_z and a_x (defined as $a_\alpha \equiv R\rho_0\sigma_\alpha$) are shown as functions of $\langle S \rangle$ for rods with $L = 200R$ and for which $\xi = 0.2R$. The volume fraction ϕ equals 0.02 and $\rho_f R/\rho_0$ equals 1 (unity), in all cases. The solid and broken curves display the longitudinal and transverse conductivities, respectively. For each set of curves (solid and broken), from top to bottom (viewed at the right-hand side of the figure where $\langle S \rangle$ approaches unity), the ODFs used are the step function ODF (iii) (topmost); ODF (i) for which σ_S equals zero (middle); and ODF (ii) for which $\sigma_S = \sigma_S^{max}$ (lowermost).

III. RESULTS

We next present results for the longitudinal and transverse conductivities as functions of the orientational order parameter, obtained from calculations that use the model described in the foregoing sections. In all cases, we assume that $L = 200R$ and $\xi = 0.2R$ for the rods, which correspond to a length of $\approx 1\,\mu$m, diameter of ≈ 10 nm, and tunneling length of ≈ 1 nm. The remaining variables in the problem are the volume fraction ϕ, the mean value of the orientational order parameter $\langle S \rangle$, the choice of ODF, and the dimensionless quantity $\rho_f R/\rho_0$. For each combination of these quantities, we first use the results from Sec. II C. to calculate the required orientational averages over trigonometric functions. These results are then used with Eqs. (2) and (3) to determine the threshold value for λ_c/R, and the conductivities are then calculated from Eq. (9).

Figures 1 and 2 present results for the longitudinal and transverse conductivities, and for the anisotropy ratio σ_z/σ_x, as functions of $\langle S \rangle$ for each of the three ODFs with $\rho_f R/\rho_0$ held fixed at the value of 1 (unity). The anisotropy ratio (Fig. 2), and the transverse conductivity (dashed lines in Fig. 1), are found to monotonically increase, and decrease, respectively, as functions of $\langle S \rangle$ for each of the ODFs investigated. As a function of increasing $\langle S \rangle$, the longitudinal conductivity (solid lines in Fig. 1) first rises gradually toward a peak and then shows a steep decline as perfect alignment is approached. The solid and dashed curves in Fig. 1 corresponding to ODFs (i) and (ii) do not merge with each other as $\langle S \rangle$ approaches zero, because these ODFs do not recover the isotropic distribution in this limit. For the same reason, the anisotropy ratio (Fig. 2) approaches unity when $\langle S \rangle$ approaches zero only for the step function ODF
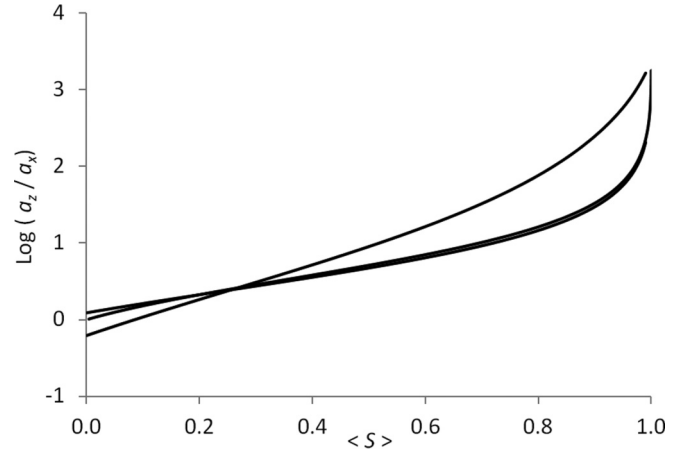

FIG. 2. The anisotropy ratios between longitudinal and transverse conductivities a_z and a_x ($a_z/a_x \equiv \sigma_z/\sigma_x$) are shown as functions of $\langle S \rangle$ for rods with $L = 200R$ and for which $\xi = 0.2R$. The volume fraction ϕ equals 0.02 and $\rho_f R/\rho_0$ equals 1 (unity), in all cases. From top to bottom (viewed at the left-hand side of the figure where $\langle S \rangle$ approaches zero), the ODFs used are ODF (i) for which σ_S equals zero (topmost); the step function ODF (iii) (middle); and ODF (ii) for which $\sigma_S = \sigma_S^{max}$ (lowermost).

[ODF (iii)]. The associated connectedness ranges or soft-shell thicknesses λ_c/R that ensure that the percolation threshold condition [Eq. (3)] is fulfilled are shown in Fig. 3. For the ODFs for which $\sigma_S = \sigma_S^{max}$ and $\sigma_S =$ zero [ODFs (i) and (ii)], λ_c/R is a monotonically increasing function of the degree of particle alignment; for the step function ODF [ODF (iii)], λ_c/R shows a very shallow minimum at $\langle S \rangle \approx 0.09$, followed by a subsequent monotonic increase. The peaks in the longitudinal conductivity (Fig. 1) thus arise in spite of (rather than as a consequence of) the trend of variation in the net displacement in the field direction per tunneling event, which
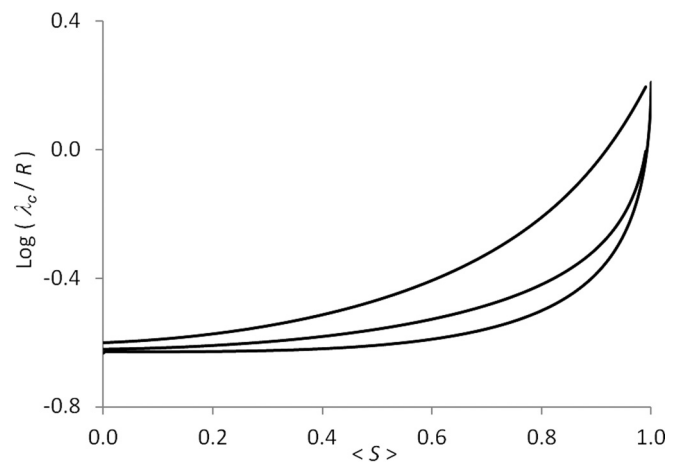

FIG. 3. The critical values of the connectedness range λ_c/R at the percolation threshold are shown as functions of $\langle S \rangle$ for rods with $L = 200R$ and for which $\xi = 0.2R$. The volume fraction ϕ equals 0.02 and $\rho_f R/\rho_0$ equals 1 (unity), in all cases. From top to bottom, the ODFs used are ODF (ii) for which $\sigma_S = \sigma_S^{max}$ (topmost); ODF (i) for which σ_S equals zero (middle); and the step function ODF (iii) (lowermost).
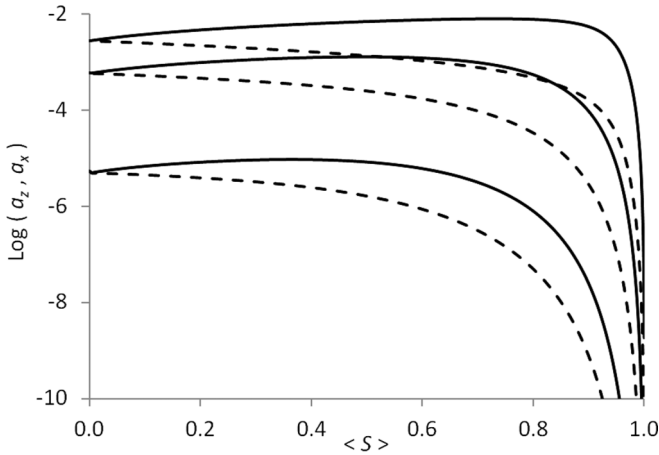
FIG. 4. The nondimensionalized longitudinal and transverse conductivities a_z and a_x (defined as $a_\alpha \equiv R\rho_0\sigma_\alpha$) are shown as functions of $\langle S \rangle$ for rods with $L = 200R$ and for which $\xi = 0.2R$. In all cases, we have used the step function ODF [ODF (iii)] and $\rho_f R/\rho_0$ equals 1 (unity). The solid and broken curves display the longitudinal and transverse conductivities, respectively. For each set of curves (solid and broken), from top to bottom, the volume fraction ϕ equals 0.04, 0.02, and 0.01.
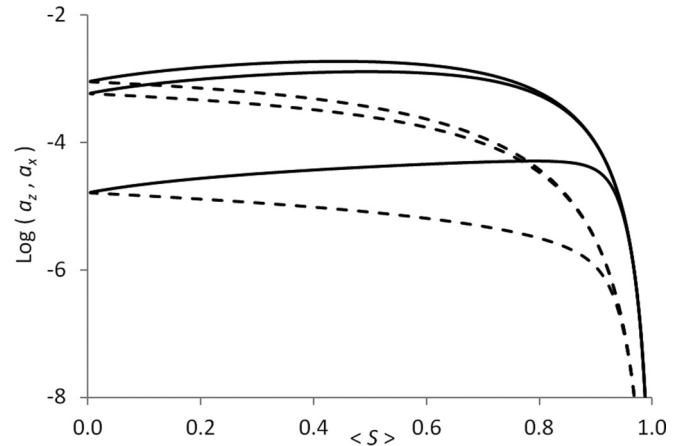

FIG. 5. The nondimensionalized longitudinal and transverse conductivities a_z and a_x (defined as $a_\alpha \equiv R\rho_0\sigma_\alpha$) are shown as functions of $\langle S \rangle$ for rods with $L = 200R$ and for which $\xi = 0.2R$. In all cases, we have used the step function ODF [ODF (iii)] and ϕ equals 0.02. The solid and broken curves display the longitudinal and transverse conductivities, respectively. For each set of curves (solid and broken), from top to bottom, $\rho_f R/\rho_0$ equals 0.01, 1, and 100.

our model assumes to be equal to λ_c. (For the solid curve in Fig. 1 that corresponds to the step function ODF [ODF (iii)], the peak in σ_z occurs at approximately $\langle S \rangle \approx 0.49$, which is in a region where λ_c/R is an increasing function of $\langle S \rangle$). Similar peaks and nonmonotonic behavior in σ_z as a function of $\langle S \rangle$ have been reported in experiments [15], and by simulations that have employed the step function ODF [19,20]. Our results suggest that this observation may not be limited to the step function ODF alone, and could be a more general phenomenon that is not especially sensitive to the details of the applicable ODF. It should be noted in addition (although perhaps obvious from inspection of Fig. 1) that the conductivities depend upon the choice of ODF, or in other words, specification of $\langle S \rangle$ alone is insufficient to uniquely determine the values of the σ_α.

Increasing the degree of alignment of the particles (increasing $\langle S \rangle$) leads to a rise in tunneling distance λ_c for each step between rods that, in turn, translates into a larger resistance (smaller conductance) for each such event. Additionally, enhanced alignment leads to a decrease (increase) in the projected distance traveled along the particle axis in directions transverse (longitudinal) to the alignment direction, and therefore to more (fewer) steps between rods required for current transfer across the same net displacement in these directions. The competition and interplay between these phenomena are what (within the present model) lead to the emergence of a peak in the longitudinal conductivity, while the transverse conductivity remains a monotonically decreasing function of $\langle S \rangle$ (Fig. 1).

The impact of varying ϕ and $\rho_f R/\rho_0$, with other parameters kept fixed, is examined in Figs. 4 and 5 for the choice of the step function ODF [ODF (iii)]. [Qualitatively similar results are found for ODFs (i) and (ii)]. The dependence upon ϕ when $\rho_f R/\rho_0$ is held fixed at unity is shown in Fig. 4; increasing volume fractions are found to always lead

to greater conductivities in both longitudinal and transverse directions. Interestingly, the peak in the longitudinal conductivity shifts toward larger values of $\langle S \rangle$ with rising particle volume fractions, in a trend that is qualitatively similar to one that has been noted in computer simulations [19,20]. Figure 5 shows the effects of altering $\rho_f R/\rho_0$ at a fixed volume fraction; an increase in $\rho_f R/\rho_0$ can be interpreted as an increase in the lineal resistivity of the rods for a constant value of the tunneling resistance between rods at contact. Increasing $\rho_f R/\rho_0$ is found to lower $R\rho_0\sigma$ in both longitudinal and transverse directions, and the peak in the longitudinal conductivity moves toward larger values of $\langle S \rangle$.

IV. CONCLUDING REMARKS

A lattice analog for percolation by rods in the continuum has been integrated with a simple-minded and heuristic model of resistors in series and parallel to describe conductivity anisotropies in nanocomposites comprising an insulating matrix and partially aligned, conducting, fibers. Calculations performed for three different choices of orientational distribution function each reveal a nonmonotonic dependence of the longitudinal conductivity σ_z upon the mean orientational order parameter $\langle S \rangle$. The transverse conductivity σ_x, by contrast, declines monotonically with increasing $\langle S \rangle$ in each instance. The location of the peak in σ_z shifts toward higher degrees of particle alignment with increasing particle volume fractions, consistent with a qualitative pattern that has been observed in more sophisticated computer simulation–based investigations [19,20]. Our findings additionally reveal the importance of modeling the entire orientational distribution as opposed to accounting for $\langle S \rangle$ alone, as the absolute values of the conductivities are shown to be sensitive to the shape and nature of the ODF (Fig. 1) and thereby to higher moments of the order parameter. Although the present work examined the simplest case of monodisperse, randomly located

particles, the underlying percolation theory has been generalized to treat polydisperse and correlated-particle systems as well [38]. Considering the impact of these additional variables that permit a more realistic modeling of the state of dispersion will be a focus of our future efforts.

[1] D. Stauffer and A. Aharony, *Introduction to Percolation Theory* (Taylor & Francis, London, 1991).

[2] S. Torquato, *Random Heterogeneous Materials: Microstructure and Macroscopic Properties* (Springer, New York, 2002).

[3] S. Kirkpatrick, Rev. Mod. Phys. **45**, 574 (1973).

[4] R. Zallen, *The Physics of Amorphous Solids* (John Wiley and Sons, New York, 1983).

[5] R. Albert and A. L. Barabasi, Rev. Mod. Phys. **74**, 47 (2002).

[6] M. E. J. Newman, S. H. Strogatz, and D. J. Watts, Phys. Rev. E **64**, 026118 (2001).

[7] J. Ren, L. Zhang, and S. Siegmund, Sci. Rep. **6**, 22420 (2016).

[8] S. I. White, R. M. Mutiso, P. M. Vora, D. Jahnke, S. Hsu, J. M. Kikkawa, J. Li, J. E. Fischer, and K. I. Winey, Adv. Funct. Mater. **20**, 2709 (2010).

[9] R. M. Mutiso, M. C. Sherrott, J. Li, and K. I. Winey, Phys. Rev. B **86**, 214306 (2012).

[10] J. Sapkota, A. Gooneie, A. Shirole, and J. Cesar Martinez Garcia, J. Appl. Polym. Sci. **134**, 45279 (2017).

[11] J. R. Capadona, O. Van Den Berg, L. A. Capadona, M. Schroeter, S. J. Rowan, D. J. Tyler, and C. Weder Nat. Nanotechnol. **2**, 765 (2007).

[12] S. Y. Kwon, I. M. Kwon, Y.-G. Kim, S. Lee, and Y.-S. Seo, Carbon **55**, 285 (2013).

[13] S. V. Ahir, A. M. Squires, A. R. Tajbakhsh, and E. M. Terentjev, Phys. Rev. B **73**, 085420 (2006).

[14] W. A. Chapkin, J. K. Wenderott, P. F. Green, and A. I. Taub, Carbon **131**, 275 (2018).

[15] F. Du, J. E. Fischer, and K. I. Winey, Phys. Rev. B **72**, 121404(R) (2005).

[16] S. I. White, B. A. DiDonna, M. Mu, T. C. Lubensky, and K. I. Winey, Phys. Rev. B **79**, 024301 (2009).

[17] X. Li, J. Cai, Y. Shi, Y. Yue, and D. Zhang, ACS Appl. Mater. Interfaces **9**, 1593 (2017).

[18] J. Wan, J. Song, Z. Yang, D. Kirsch, C. Jia, R. Xu, J. Dai, M. Zhu, L. Xu, C. Chen, Y. Wang, Y. Wang, E. Hitz, S. D. Lacey, Y. Li, B. Yang, and L. Hu, Adv. Mater. **29**, 1703331 (2017).

[19] S. Gong, Z. H. Zhu, and S. A. Meguid, Polymer **56**, 498 (2015).

[20] W. S. Bao, S. A. Meguid, Z. H. Zhu, and M. J. Meguid, Nanotechnology **22**, 485704 (2011).

[21] A. P. Chatterjee, J. Chem. Phys. **132**, 224905 (2010).

[22] A. P. Chatterjee, J. Chem. Phys. **140**, 204911 (2014).

[23] V. Ambegaokar, B. I. Halperin, and J. S. Langer, Phys. Rev. B **4**, 2612 (1971).

[24] J. E. Fischer, W. Zhou, J. Vavro, M. C. Llaguno, C. Guthy, R. Haggenmueller, M. J. Casavant, D. E. Walters, and R. E. Smalley, J. Appl. Phys. **93**, 2157 (2003).

[25] C. Zamora-Ledezma, C. Blanc, N. Puech, M. Maugey, C. Zakri, E. Anglaret, and P. Poulin, Phys. Rev. E **84**, 062701 (2011).

[26] M. Weber and M. R. Kamal, Polym. Compos. **18**, 711 (1997).

[27] R. H. J. Otten and P. van der Schoot, Phys. Rev. Lett. **103**, 225704 (2009).

[28] R. H. J. Otten and P. van der Schoot, J. Chem. Phys. **134**, 094902 (2011).

[29] K. Leung and D. Chandler, J. Stat. Phys. **63**, 837 (1991).

[30] M. C. Hermant, B. Klumperman, A. V. Kyrylyuk, P. van der Schoot, and C. E. Koning, Soft Matter **5**, 878 (2009).

[31] B. Nigro and C. Grimaldi, Phys. Rev. B **90**, 094202 (2014).

[32] A. P. Philipse, Langmuir **12**, 1127 (1996).

[33] L. Onsager, Ann. N. Y. Acad. Sci. **51**, 627 (1949).

[34] Equation (3) of Ref. [22].

[35] M. E. Fisher and J. W. Essam, J. Math. Phys. **2**, 609 (1961).

[36] S.-Y. Fu and B. Lauke, Compos. Sci. Technol. **56**, 1179 (1996).

[37] W. S. Bao, S. A. Meguid, Z. H. Zhu, and G. J. Weng, J. Appl. Phys. **111**, 093726 (2012).

[38] A. P. Chatterjee, J. Chem. Phys. **137**, 134903 (2012).